

Nazarii Danyliuk¹, Ivanna Lapchuk¹, Volodymyr Kotsyubynsky²,
Volodymyra Boychuk², Viktor Husak³

Effect of Mn²⁺ substitution on catalytic properties of Fe_{3-x}Mn_xO₄ nanoparticles synthesized via co-precipitation method

¹Educational and Scientific Center of Material Science and Nanotechnology, Vasyl Stefanyk Precarpathian National University, Ivano-Frankivsk, Ukraine, danyliuk.nazariy@gmail.com

²Department of Material Science and New Technology, Vasyl Stefanyk Precarpathian National University, Ivano-Frankivsk, Ukraine, kotsyubynsky@gmail.com

³Department of Biochemistry and Biotechnology, Vasyl Stefanyk Precarpathian National University, Ivano-Frankivsk, Ukraine, gus_net@ukr.net

Mn-substituted magnetite samples Fe_{3-x}Mn_xO₄ (x = 0.0; 0.02; 0.05; 0.1; 0.15; 0.2; 0.25) were synthesized using the co-precipitation method. X-ray diffraction patterns confirmed the formation of pure, well-crystallized manganese ferrite with a cubic spinel structure. The crystallites size increases sharply for the minimum degrees of substitution, with a subsequent tendency to decrease with the growth of manganese ions content. The catalytic properties of Fe_{3-x}Mn_xO₄ were investigated for the degradation of oxytetracycline (OTC) and inactivate *E. coli*. There is a correlation between particle size and catalytic activity. The Fe_{2.95}Mn_{0.05}O₄ sample exhibited the highest catalytic activity in the destruction of OTC. The effect of electromagnetic heating (EMH) on the catalytic properties of iron oxides were investigated. The Fe_{2.9}Mn_{0.1}O₄ sample with electromagnetic heating achieved 100 % efficiency in decomposing 5 mg/L of OTC. Fe_{3-x}Mn_xO₄ samples reduce the number of Gram-negative bacteria *E. coli* at concentrations of 10⁴ and 10⁶ CFU/mL. Electromagnetic heating experiments demonstrated high performance, achieving inactivation of 6 logs of *E. coli* in the presence of Fe_{2.98}Mn_{0.02}O₄ and Fe_{2.95}Mn_{0.05}O₄ catalysts within 135 minutes. Studies on ecotoxicity have shown that *Daphnia magna* is a sensitive bioindicator of residual H₂O₂ concentration. An increase in the Mn²⁺ content in the synthesized catalysts resulted in a decrease in the toxicity of purified water. The study suggests that Mn-substituted magnetite catalysts are effective materials for catalytic decomposition of OTC and inactivation of *E. coli* bacteria.

Key words: catalyst, Mn-substituted magnetite, hydrogen peroxide, electromagnetic heating, *E. coli*, *Daphnia magna*.

Received 17 August 2023; Accepted 20 December 2023.

Introduction

One of important scientific problems is the wastewater treatment from persistent organic pollutants, which have increased molecular weight and hydrophobic properties. Such materials include pharmaceuticals and agrochemicals, which tend to accumulate in environmental food chains. The presence of pharmaceuticals in wastewater may be dangerous because they directly affect aquatic organisms. For example, the number of antibiotic-resistant bacteria increases every

year. Antibiotic-resistant microorganisms are dangerous because they can cause the rapid spread of infectious diseases among people.

To avoid the negative impact of persistent pollutants, improved water purification and disinfection technologies are needed [1]. Advanced oxidation processes (AOP) are highly effective technologies for removing organic pollutants [2]. The Fenton reaction generates hydroxyl radicals from the decomposition of hydrogen peroxide using an iron-based catalyst. Due to its high oxidative potential (of 2.8 V), hydroxyl radicals rapidly destroy

organic and biological pollutants [3].

Nanoparticles of iron oxides are known as active catalytic materials in Fenton processes for the destruction of a wide range of pollutants. Iron oxides are considered promising catalysts due to their availability in the earth's crust, high stability and low solubility in water [4]. Among iron oxides, magnetite, hematite, and maghemite are the most active heterogeneous catalysts for water purification [1,5,6]. A comparative study on the catalytic properties of maghemite, magnetite, and goethite mixed with silica was carried out using methyl red (MR) and H₂O₂ at pH values of 5 and 7 [7]. It was found, that the catalytic activity depends on the degree of iron oxidation. Catalytic properties of iron oxide materials depend also on crystal structure, surface area, size and volume of pores and inclusion of additional metal atoms [8].

Doping with transition metals is an effective way to improve activity of heterogeneous Fenton catalysts. For example, manganese ions are used to adjust the structural and morphological characteristics of catalysts [9,10]. Porous nanoparticles (Mn_xFe_{3-x}O₄) with varying molar ratios of Mn/Fe were synthesized for the degradation of sulfamethoxazole (SMX) [10]. The antibiotic was degraded by the dissociation of peroxymonosulfate (PMS) to form free radicals SO₄^{•-}, •OH, and singlet oxygen ¹O₂. With an increase in the manganese content, the degradation efficiency of SMX increased from 19 to 70% for 30 minutes. The synthesized manganese ferrite nanoparticles can sustain high degradation efficiency of SMX over five degradation cycles. The synthesis of a high-efficiency composite catalyst of reduced graphene oxide/MnFe₂O₄ (RGO/MnFe₂O₄) for the decomposition of methylene blue (MB) using the Hummers method is described in the paper [11]. A 50 mg/L MB solution can be completely decolorized in 130 minutes and mineralized by 78% using 5 mg of RGO/MnFe₂O₄ in the presence of H₂O₂ at room temperature. In the catalytic reactions, the initial stage (< 70 min) is dominated by the Fe³⁺/Fe²⁺ redox process, while the second stage (>70 min) involves Mn³⁺/Mn²⁺.

MnFe₂O₄ nanoparticles and MnFe₂O₄/biochar composite with different biochar content were prepared for hydrogen peroxide activation for tetracycline (TC) degradation [12]. Under visible light irradiation in the presence of 100 mmol/L H₂O₂ for 2 hours, the MnFe₂O₄/biochar composite demonstrated 95% decomposition of 40 mg/L TC as a heterogeneous Fenton photocatalyst. XPS measurements indicate that the activation of H₂O₂ involves Fe and Mn ions. Biochar inhibits the aggregation of MnFe₂O₄ nanoparticles, thereby enhancing the efficiency of TC removal. Chen et al. [13] synthesized a new hybrid of Mn-doped Fe₃O₄ magnetic microspheres combined with reduced graphene oxide (Mn-Fe₃O₄/RGO) employing the solvothermal method. The prepared Mn-Fe₃O₄/RGO was used as a heterogeneous photo-Fenton catalyst for the decomposition of Rhodamine B (RhB). A high degradation efficiency of RhB (approximately 96.4%) is observed with a low catalyst dosage of 0.2 g/L in the presence of H₂O₂ for 80 minutes under UV irradiation. Magnetic catalyst retains high efficiency of approximately 90% after ten cycles of dye degradation. The catalyst is easily separated from the solution by an external magnetic

field. Synthesized Mn_{1.8}Fe_{1.2}O₄ nanospheres as activators of peroxymonosulfate (PMS) for the degradation of bisphenol A (BPA) are described in paper [14]. Due to the synergistic effect between metal cations of bimetallic oxides, the nanospheres demonstrated excellent performance in a wide pH range from 4 to 10. It has been found that Mn is an active center on the surface of the Mn_{1.8}Fe_{1.2}O₄ nanospheres. However, Fe(III) serves as the primary adsorption site for reaction substrates. Sulfate and hydroxyl radicals were formed during the activation of PMS. In this work [15], describes the synthesis of a Fe₃O₄@MnO₂ nanocomposite for purifying water contaminated with Rhodamine B (RhB) and *Escherichia coli* (*E. coli*). The Fe₃O₄@MnO₂ nanocomposite exhibited high photocatalytic activity. Pathogenic *E. coli* bacteria were inactivated after 90 minutes of irradiation. The efficiency of RhB photodegradation was 75%. The study demonstrates that catalysts containing manganese exhibit photocatalytic properties against pathogenic bacteria and effectively eliminate organic toxicants. Thus, manganese doping into iron oxides increases their catalytic activity in both bacterial inactivation and organic pollutant decomposition.

I. Experimental

1.1. Synthesis of Mn-substituted magnetite

In this work, Fe_{3-x}Mn_xO₄ catalysts were synthesized by the co-precipitation method. The salts FeCl₃•6H₂O, FeCl₂•4H₂O, and MnSO₄•H₂O are sources of Fe³⁺, Fe²⁺, and Mn²⁺ ions, respectively. The synthesis Mn-doped magnetite was carried out with different molar ratios of manganese (II) and iron (II): 0.0:1.0; 0.02:0.98; 0.05:0.95; 0.1:0.9; 0.15:0.85; 0.2:0.8 and 0.25:0.75, labeled as: Mn-00, Mn-02, Mn-05, Mn-10, Mn-15, Mn-20 and Mn-25. The salts were dissolved in 500 mL of distilled water and stirred thoroughly with a top-drive stirrer at 600 rpm for 30 minutes. The mixture was then heated to 90°C in a water bath. A precipitating agent of NaOH with a concentration of 5 M and a volume of 500 mL was added using a burette over a period of 2.5 hours. The reaction temperature and stirring speed were maintained at 90°C and 600 rpm, respectively. The synthesized ferrites were washed with distilled water until the pH reached 7. The Fe_{3-x}Mn_xO₄ samples were then dried at 60°C.

1.2. Characterization methods

The structures of the synthesized ferrites samples were examined by X-ray powder diffraction method (Shimadzu XRD-7000 X-ray diffractometer) using Cu K α monochromatic radiation source ($\lambda = 0.15406$ nm) and a graphite monochromator operating at 40 kV and 30 mA at room temperature. A LaB₆ 660c reference sample was used as a standard for microstructural analysis. Match 3.0 software was utilized for crystal phases identification.

The ⁵⁷Fe Mössbauer spectra were recorded using an MS1104EM spectrometer at constant acceleration regimes with a ⁵⁷Co source within a Cr matrix (activity of about 8 mCi). Isomer shifts were calibrated relative to α -Fe at room temperature. Hyperfine interaction parameters were calculated using the Univem software.

1.3. Catalytic wet peroxide degradation of oxytetracycline

The experiment on the catalytic degradation of OTC was carried out at 20 °C in a glass reactor. The reaction system (120 mg of catalyst and 40 mL of 5 mg/L OTC solution) was stirred for 30 min to achieve adsorption-desorption equilibrium. Catalytic reaction was initiated by the addition of H₂O₂ (10 mM). At regular intervals, 1.5 mL of the reaction solution was taken to analyze the residual OTC concentration using a ULAB 102-UV spectrophotometer. The residual concentration of OTC was determined by spectrophotometric method at 356 nm. The OTC concentration was calculated by equation: $C_x = A_x/0.0282$ [16]. The most active samples of Fe_{2.95}Mn_{0.05}O₄ and Fe_{2.9}Mn_{0.1}O₄ were studied in more detail by changing the concentration of OTC (3, 5, 7, 10 mg/L) and the concentration of H₂O₂ (10, 20, and 30 mM). The experiments were performed without and with electromagnetic heating (31.4 V, 7.86 A, 100 kHz) [17]. The residual concentration of H₂O₂ was analyzed by the metavanadate method. The measuring absorbance solution at 470 nm with a ULAB 102-UV spectrophotometer. The H₂O₂ concentration was calculated by equation: $C_x = A_x/0.29917$ [17]. All experimental data on OTC degradation were averages of three replicates. The OTC degradation efficiency was determined using the following equation:

$$\text{Degradation efficiency OTC (\%)} = \frac{(C_0 - C_t)}{C_0} * 100\% \quad (1)$$

where C₀ - initial concentration of OTC, C_t - residual concentration of OTC in solution at time t. The kinetics of OTC degradation was analyzed using a first-order model. In this work, the experimental rate constants of OTC degradation were determined. The first-order equation is as follows: $\ln([\text{OTC}]_t/[\text{OTC}]_0) = -k[\text{OTC}] * t$, where k[OTC] is the experimental rate constant of the reaction, and [OTC]_t and [OTC]₀ are the concentrations of OTC in the solution at time t and 0 min, respectively.

1.4. Bacterial inactivation tests

The number of *E. coli* bacteria was determined through experiments using the membrane filtration method. Gram-negative *E. coli* (ATCC 35218) were inoculated into sterile medium in Petri dishes and grown under optimal conditions (37°C for 24 h). Bacterial suspensions were prepared from formed colonies by serial dilutions to achieve concentrations of 10⁴ CFU/mL and 10⁶ CFU/mL. For the experiment on the catalytic inactivation of *E. coli*, we used a batch reactor with a volume of 100 mL and a laboratory shaker. The weights of Fe_{3-x}Mn_xO₄, where x = 0.0, 0.02, 0.05, 0.1, 0.15, 0.2, and 0.25 were 1 g/L and 3 g/L. The hydrogen peroxide concentrations were 10 mM and 20 mM. After conducting the experiment, samples of water were collected for sowing on membrane filters. The treated water aliquots were sampled at 0, 10, 25, 45, 75, 105, and 135 minutes. Membrane filters measuring 35 mm in diameter and with a pore size of 0.9 μm were placed on Petri dishes containing Endo medium, and incubated at 37°C for one day. Control experiments were conducted. The number of residual dark red *E. coli* colonies that grew on the

membrane filters was quantified.

2.5 Ecotoxicity bioassays

The acute ecotoxicity of water using *Daphnia magna* organisms was assessed according to the method described in ISO 6341:2012 [18]. Ten neonates (6-24 hours) were used for each of the three replicates. All tests were performed at 20±2°C. Number of immobile organisms was recorded after 24 and 48 hours. The control solution was settled water. The results were expressed as a mortality rate in % and the EC50 values were calculated for 24 and 48 hours of exposure. The analysis ecotoxicity of water was performed under experimental conditions: [E. coli]₀ = 10⁶ CFU/mL; [catalyst]₀ = 3 g/L; [H₂O₂]₀ = 20 mM.

II. Results and discussion

2.1. Structure characterization XRD

The X-ray diffraction patterns of the synthesized ferrite powders are shown in Fig. 1a. All peaks are indexed to the spinel cubic structure confirming the formation of pure well-crystallized manganese ferrite. The any impurity absence indicating the successful application of synthesis method to obtaining of manganese ferrite nanoparticles. Observed reflections corresponds to the lattice planes of (111), (220), (311), (222), (400), (422), (333), (440) of ferrite spinel structure (JCPDS # 74-2403). Rietveld refinement by using FullProf software was used for XRD data analysis. Lattice parameters of Fe_{3-x}Mn_xO₄. The growth of lattice constant (a) for synthesized ferrites with manganese content growth is observed (Fig. 1b). The spinel structure belongs to the Fd-3m space group (225 symmetry group) where 32 oxygen ions form a cubic close-packed framework forming of tetrahedral and octahedral sites (A- and B-sites, respectively). The bulk manganese ferrite typically has normal arrangement where Mn²⁺ ions are located in A sites and Fe³⁺ ions are distributed in B sites. For ultrafine manganese ferrite mixed structure was observed repeatedly [19,20] (Mn_{1-δ}Fe_δ)_A[Mn_δFe_{2-δ}]_BO₄, where the inversion degree δ parameter describes the number of divalent ions in octahedral (B) positions. Previously the effect of inversion degree on crystallite size and catalytic activity of nanosized cobalt ferrites was reported [21]. At the same time the respectively narrow range of Mn-substitution (0 ≤ x ≤ 0.25) allows to state that the localization of manganese ions in the tetrahedral positions of the spinel lattice will be the dominant. The lattice constant a of (Mn_xFe_{1-x})_A[Fe₂]_BO₄ ferrites was calculated using the Rietveld refinement. The increase in the lattice parameter with manganese ions concentration growth (Pearson's correlation coefficient is r = 0.863) corresponds is predictable and is explained within the close-packing model of spinel structure formation by the relatively larger size of tetrahedrally coordinated manganese ions (0.66 Å) [22] compared to the ionic radius of iron ions (0.49 Å) [23]. The substitution degree (x) growth causes the changes of the full width at half maximum (FWHM) than correspond to crystallite size variation (Fig. 1c). The most intense (311) reflexes of patterns were used for calculation the average crystallite size (D_s) of ferrites accordingly to

the Scherrer's formulae: $D_S = \frac{K_S \lambda}{\beta \cos \theta}$, λ is the X-ray wavelength; β is the reflex broadening; θ is the Bragg's angle, $K_S = 0.89$ for spherical crystallites. The line broadening β was calculated as $\beta = \sqrt{\beta_{exp}^2 - \beta_i^2}$, where β_i and β_{exp} are the FWHM values of the instrumental line and (311) peak, respectively. It was found that the crystallites

size increases sharply for the minimum degrees of substitution, with a subsequent tendency to decrease with the growth of manganese ions content (Fig. 1d). For obtained results verification and the consideration of strain effects on the diffraction profiles size-strain plot (SSP) method was applied [24]. The SSP analysis is based on the linearization of next equation plot:

$$(d_{hkl} \beta_{hkl} \cos(\theta) / \lambda)^2 = \frac{K_{SSP}}{D_{SSP}} (d_{hkl})^2 \beta_{hkl} \cos(\theta) / \lambda + (2\varepsilon)^2,$$

where D_{SSP} is average crystallite size, d_{hkl} is the interplanar spacing for (hkl) plane, ε the intrinsic strain, and K_{SSP} equals of 0.75 for spherical crystallite. The obtained data about D_{SSP} and ε dependence on the substitution degree are plotted on Fig. 1d. The calculated D_{SSP} are expectedly smaller comparatively to the D_S (Fig. 1c) but the general regularities of crystallite sizes with the increasing of manganese content is an evidence of the applied approach correctness. The growth tendency of microstrain ε values in $(Mn_x Fe_{1-x})_A [Fe_2]_B O_4$ nanopowders with the increasing for substitution degree was observed (Fig. 1d). In our case the ε values can be considered proportional to the particle agglomeration degree. The correlation with $r = 0.728$ between x and ε values is observed.

2.2. Mossbauer spectroscopy

Room-temperature ($T = 293 \pm 2$ K) Mossbauer spectra for $(Mn_x Fe_{1-x})_A [Fe_2]_B O_4$ samples are shown in Fig. 3. All obtained spectra are formed by broadened sextets without central doublet that is an avoidance of ferrimagnetic ordering. The superparamagnetic relaxation are not observed for synthesized ferrites so the lifetime of the excited state of the ⁵⁷Fe nucleus ($\tau_{Fe} = 142$ ns) exceeds the Neel relaxation time τ_N of magnetic moment localization along the easy magnetization axes of the ferrite particle ($\tau_{Fe} \geq \tau_N$).

The Neel time is estimated from equation $\tau_N = \tau_0 \exp(K_{eff} V / (kT))$, where $\tau_0 \approx 10^{-9}$ s, K_{eff} is a constant of effective magnetocrystalline anisotropy, V is a volume of a nanoparticle, T is a temperature. Experimental data correspond to a case of $\tau_{Fe} \geq \tau_0$ which allows estimation

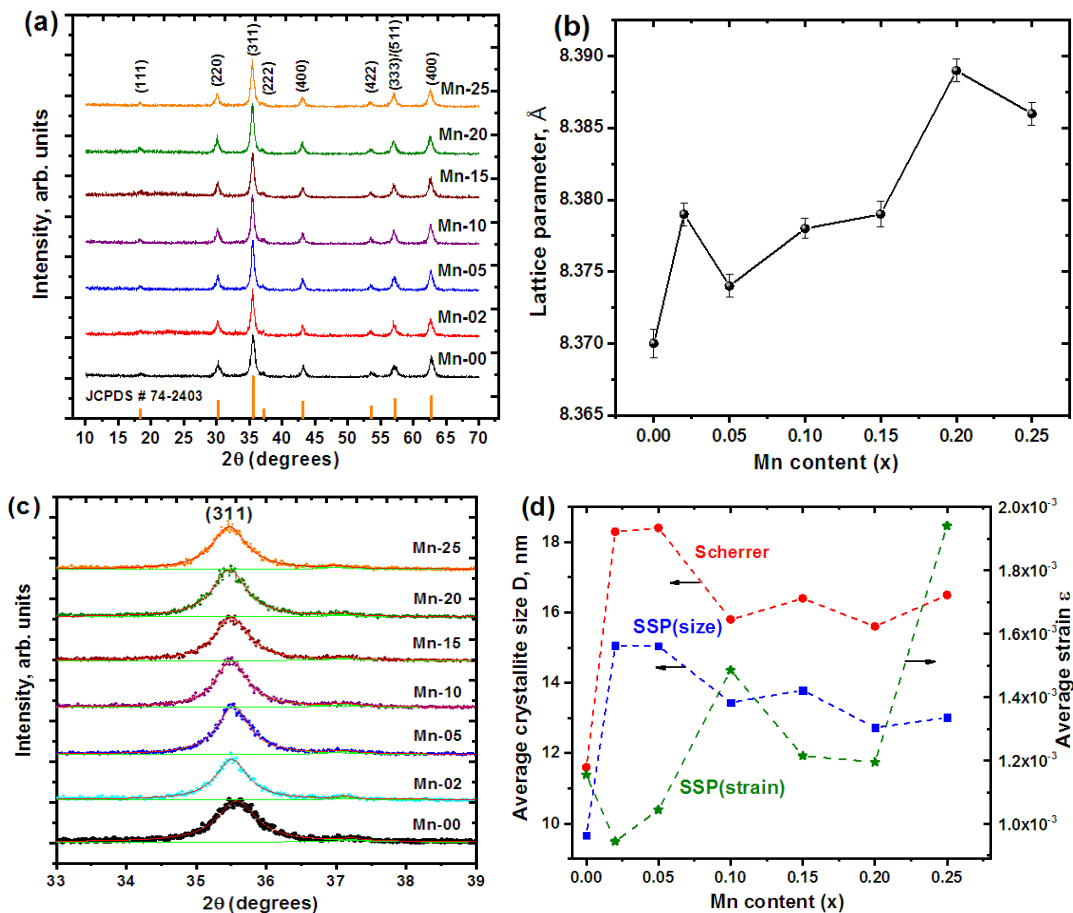


Fig. 1. (a) XRD patterns of $(Mn_x Fe_{1-x})_A [Fe_2]_B O_4$ samples; (b) lattice parameter of the ferrite samples vs. manganese content; (c) (311) reflexes broadening and (d) average crystallite size calculated by Scherrer's and SSP methods and SSP-estimated strain values as a functions of Mn²⁺ ions substitution degree (x).

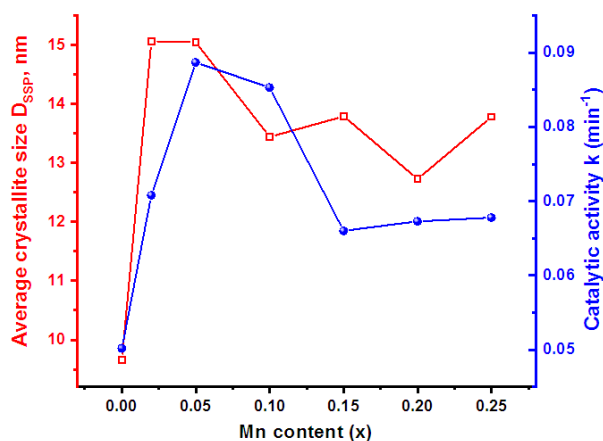


Fig. 2. The correlation between ε and a values with Pearson's correlation coefficient $r=0.750$ is observed.

of the lower limit of ferrite crystallites size. The magnetocrystalline anisotropy values of manganese ferrite can be calculated using the linear combination of the anisotropy component contribution of the all cations located in tetrahedral and octahedral sites of the spinel cubic structure: $K_{eff} = (1-x)K_{Mn}^A + xK_{Fe}^A + 2K_{Fe}^B$, where $K_{Fe}^A = -11.8 \cdot 10^5 \text{ J/m}^3$ and $K_{Fe}^B = 1.78 \cdot 10^5 \text{ J/m}^3$ [25]. The effective anisotropy constant for MnFe_2O_4 particles with an average size of 80 nm is $1.1 \cdot 10^4 \text{ J/m}^3$ [26] (for bulk MnFe_2O_4 this value is $-0.3 \cdot 10^4 \text{ J/m}^3$) [27]. The value of K_{eff} allows us to calculate $K_{Mn}^A = -3.55 \cdot 10^5 \text{ J/m}^3$. As a result the estimated values effective anisotropy constants of $(\text{Mn}_x\text{Fe}_{1-x})_A[\text{Fe}_2]_B\text{O}_4$ for x from 0 to 0.25 are in a range of $(6.1-8.2) \cdot 10^5 \text{ J/m}^3$. The estimated threshold diameter of spherical ferrite particles to superparamagnetic spherical ferrite particles using Mossbauer method is in a range of 4.2-4.6 nm that agrees with XRD data.

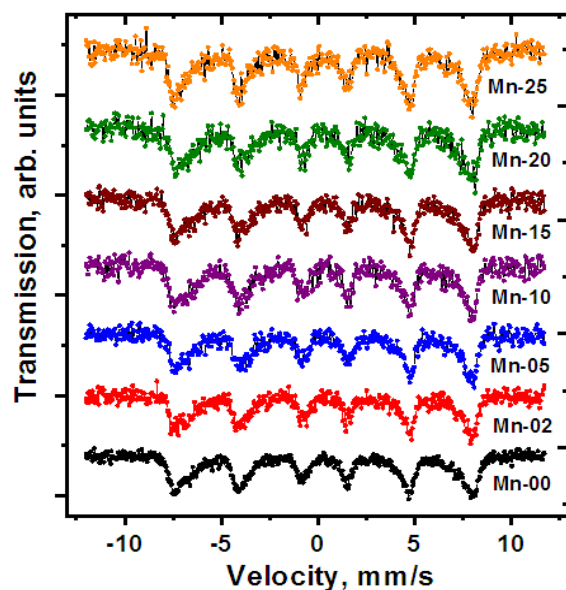


Fig. 3. Mossbauer spectra of of $(\text{Mn}_x\text{Fe}_{1-x})_A[\text{Fe}_2]_B\text{O}_4$ ferrites with manganese content $0.00 \leq x \leq 0.25$.

2.3. Catalytic activity in the wet peroxide oxidation of oxytetracycline

2.3.1. Effect of $\text{Mn}^{2+}/\text{Fe}^{2+}$ stoichiometric ratio

The degree of degradation of OTC was an important indicator for evaluating the activity of a series Mn-doped

catalysts (with different molar ratios of $\text{Mn}^{2+}/\text{Fe}^{2+}$: 0.0:1.0, 0.02:0.98, 0.05:0.95, 0.1:0.9, 0.15:0.85, 0.2:0.8, 0.25:0.75) (Fig. 4c). The results degradation of OTC with the same catalyst concentration (3.0 g/L) varied. The catalyst dose of 3 g/L was chosen for all experiments since it was sufficient for the complete decomposition of OTC in 90 minutes of reaction. All samples exhibited low adsorption capacity for OTC molecules. The degradation processes of OTC by synthesized catalysts are described using first-order kinetic models (Fig. 4 a-b). The degradation efficiency of OTC gradually increased with an increase in the stoichiometric ratio of $\text{Mn}^{2+}/\text{Fe}^{2+}$. OTC did not decompose in the reaction system without a catalyst. Only the presence of a catalyst causes the radical decomposition of H_2O_2 . H_2O_2 serves as a natural oxidizing agent in the degradation systems of OTC [28]. In the system catalyst/ H_2O_2 , OTC (5 mg/L) underwent rapid degradation during the first 10 minutes, followed by a gradual decrease in degradation efficiency. The sample that exhibited the highest activity was $\text{Fe}_{2.95}\text{Mn}_{0.05}\text{O}_4$, with a degradation rate of 86.76% and a reaction rate constant of 0.0887 min^{-1} . The $\text{Fe}_{2.9}\text{Mn}_{0.1}\text{O}_4$ sample was the second most active, with a degradation rate of 80.88% and a reaction rate constant of 0.0853 min^{-1} . The UV-visible spectra of the solutions after the degradation process of OTC by $\text{Fe}_{3-x}\text{Mn}_x\text{O}_4$ catalysts are shown in Figure 4-d. To investigate the degradation efficiency of OTC under different experimental conditions, we used the $\text{Fe}_{2.95}\text{Mn}_{0.05}\text{O}_4$ and $\text{Fe}_{2.9}\text{Mn}_{0.1}\text{O}_4$ catalysts, which exhibited the highest activity among the seven synthesized catalysts. The results suggest that the catalytic decomposition of pollutants is significantly enhanced by certain combinations of Fe^{2+} and Mn^{2+} [14,29]. The catalytic performance of catalysts is significantly improved by the close interaction between Mn^{2+} and Fe^{2+} , which increases the number of active sites for H_2O_2 activation.

2.3.2. Catalytic activity of $\text{Fe}_{2.95}\text{Mn}_{0.05}\text{O}_4$ sample

We investigated the influence of initial concentrations of OTC (3, 5, 7, 10 mg/L) and H_2O_2 (10, 20, 30 mM) as well as electromagnetic heating on the degradation efficiency of OTC. Figure 5 a-c shows the kinetic curves of OTC degradation using the $\text{Fe}_{2.95}\text{Mn}_{0.05}\text{O}_4$ catalyst with varying combinations of OTC and H_2O_2 . The removal of OTC in the presence of H_2O_2 is significantly more efficient than OTC removal by adsorption. Electromagnetic heating and a constant concentration of the catalyst $\text{Fe}_{2.95}\text{Mn}_{0.05}\text{O}_4$ (3 g/L) caused the complete degradation of OTC within 90 minutes. The removal rate increased as the H_2O_2 concentration increased from 10 to 30 mM. The first-order reaction rate constant (k) also increased from 0.1099 to 0.2390 min^{-1} , when the initial OTC concentration was 3 mg/L (Fig. 6). However, the reaction rate constant decreases from 0.2390 to 0.0574 min^{-1} as the initial OTC concentration increases from 3 to 10 mg/L, when the H_2O_2 concentration is 30 mM. A similar trend is observed for other H_2O_2 concentrations (Fig. 6). The initial concentration of OTC, which was 10 mg/L, reduced the contact area of the catalyst with H_2O_2 . As a result, the degradation efficiency of OTC decreased to 53.5%.

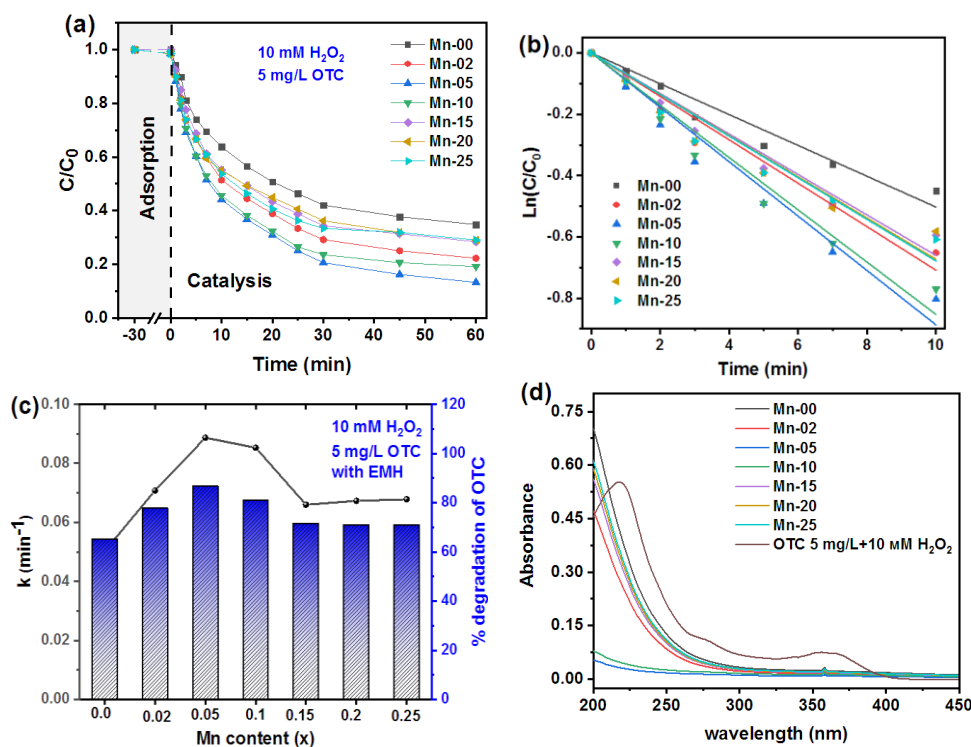


Fig. 4. (a) Catalytic activity of Fe_{3-x}Mn_xO₄ nanoparticles in the oxytetracycline decomposition; (b) log-linear transformation of the wet oxidation kinetic lines; (c) the values of wet oxidation rate constant and efficiency of OTC removal by wet peroxide oxidation catalysed with the Fe_{3-x}Mn_xO₄ samples; (d) the UV-Vis spectra for 5 mg/L OTC with H₂O₂ solutions in the presence of a Fe_{3-x}Mn_xO₄ catalysts at 298 K.

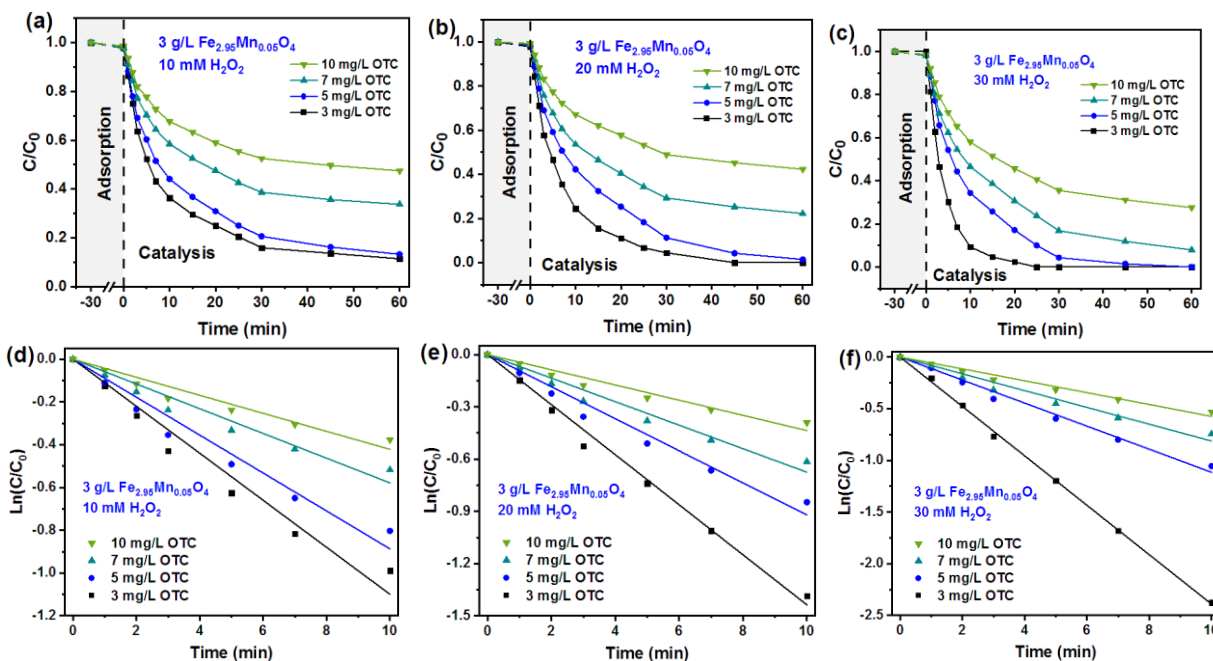


Fig. 5. (a-c) Changes of OTC concentration vs. reaction time in the presence of the Mn-05 catalyst at 298 K; (d-f) first-order kinetic model for the Mn-05 catalyst at 298 K.

The effect of electromagnetic heating was studied for a OTC concentration of 5 mg/L and H₂O₂ concentrations of 10, 20, 30 mM (Fig. 7a-b). It is worth noting that thermal activation of H₂O₂ is an effective method of generating active radicals for the decomposition of pollutants [30]. The efficiency of catalytic oxidation of OTC was improved by an increase in temperature. In addition, an increase in the concentration of H₂O₂ to

30 mM resulted in increased degradation of OTC. The reaction rate constant reached its maximum value at 0.1114 min⁻¹ when the H₂O₂ concentration was 30 mM and electromagnetic heating was applied (Fig. 7c). The Mn-05 catalyst achieved complete destruction of OTC molecules during the 90-minute reaction period. Electromagnetic heating enabled the reaction mixture to reach a temperature of 25°C. In contrast, heating the

reaction mixture to 25°C in a water bath had no discernible impact on the degradation of OTC. The efficiency of degradation 5 mg/L OTC was 100% with electromagnetic heating, 89.1% without electromagnetic heating, and 91.7% with water heating (Fig. 7d). The results show that the Mn-05 catalyst exhibits effective Fenton activity, which can be enhanced through electromagnetic heating.

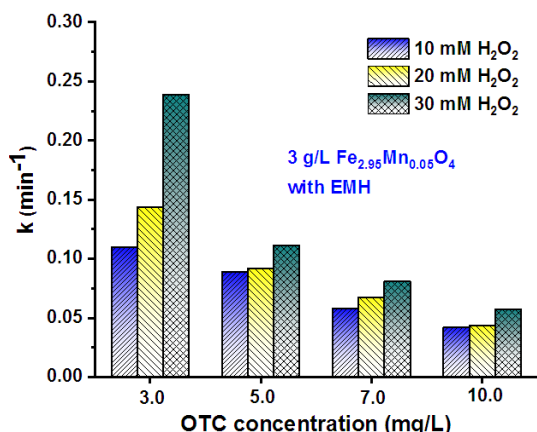


Fig. 6. Rate constants of the first-order kinetic model for the degradation of OTC with the Mn-05.

2.3.3. Catalytic activity of Fe_{2.9}Mn_{0.1}O₄ sample

The effect of OTC and H₂O₂ concentration and electromagnetic heating on the degradation of OTC was investigated using Fe_{2.9}Mn_{0.1}O₄ as a catalyst (Fig. 8). In all experiments, the OTC was destroyed after 30 minutes of adsorption time. As anticipated, a rise in the initial concentration of OTC diminishes the decomposition efficiency. The maximum efficiency of 100% can be achieved in 60 minutes when the concentration of OTC is 3 mg/L and 30 mM H₂O₂. The Mn-10 sample achieved a

degradation efficiency of 68.3% within 90 minutes at a OTC concentration of 10 mg/L and 30 mM H₂O₂. Figure 8-a shows that the catalytic activity of the Mn-10 sample was affected by the concentration of H₂O₂ (10-30 mM). The OTC degradation rate was highest when the H₂O₂ concentration was increased to 30 mM. However, even at a low H₂O₂ concentration of 10 mM, approximately 86.7% of the OTC molecules ([OTC]₀ = 3 mg/L) were removed within 60 minutes. The decrease in the density of surface-adsorbed H₂O₂ molecules likely caused a reduction in the concentration of formed radicals at the solid-liquid interface. Figure 9 shows the reaction rate constants of the Mn-10 sample at various initial concentrations of OTC ([OTC]₀ = 3-10 mg/L). The results indicate that within the test range (3-10 mg/L), at least 68.3% of OTC can be decomposed after 90 minutes and 30 mM H₂O₂, demonstrating the effectiveness of the Mn-10 catalyst in decomposing pollutants.

Under electromagnetic heating, the reaction medium reaches a temperature of 25°C. Similar to the Mn-05 sample, the degradation efficiency of OTC increases as the reaction temperature rises. Three concentrations of 10, 20, and 30 mM H₂O₂ were used to study the effect of induction heating on the decomposition efficiency of OTC (Fig. 10a-b). Figure 10c shows the calculated rate constants degradation of OTC. In the presence of 30 mM H₂O₂ and electromagnetic heating, the degradation efficiency of 5 mg/L OTC is 100% (Fig. 10d). However, when heated in a water bath at 25°C, the Mn-10 catalyst can achieve a final degradation efficiency of 86% for OTC within 90 minutes. These results demonstrate the effectiveness of electromagnetic heating in activating the catalyst for radical decomposition of H₂O₂.

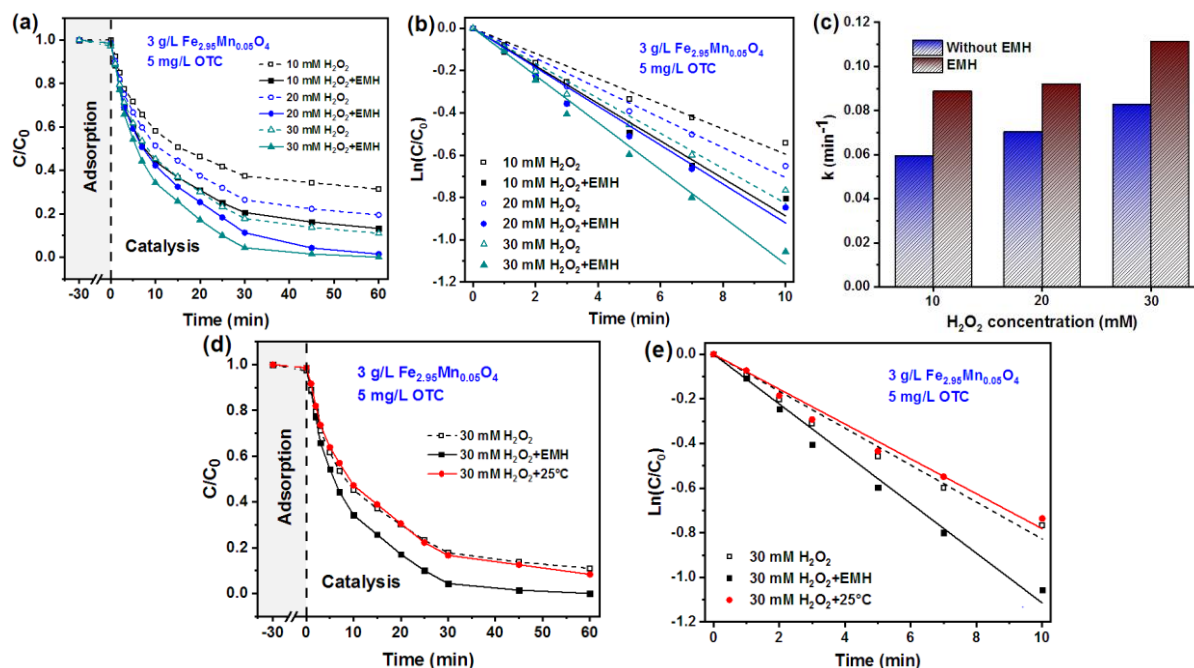


Fig. 7. (a) Catalytic activity of Mn-05 nanoparticles in the OTC decomposition without and under EMH; (b) log-linear transformation of the wet oxidation kinetic lines; (c) rate constants of the first-order kinetic model for the degradation of OTC with the Mn-05; (d) catalytic activity of Mn-05 nanoparticles in the OTC decomposition without EMH, under EMH and with heating to 25°C in a water bath; (e) log-linear transformation of the wet oxidation kinetic lines.

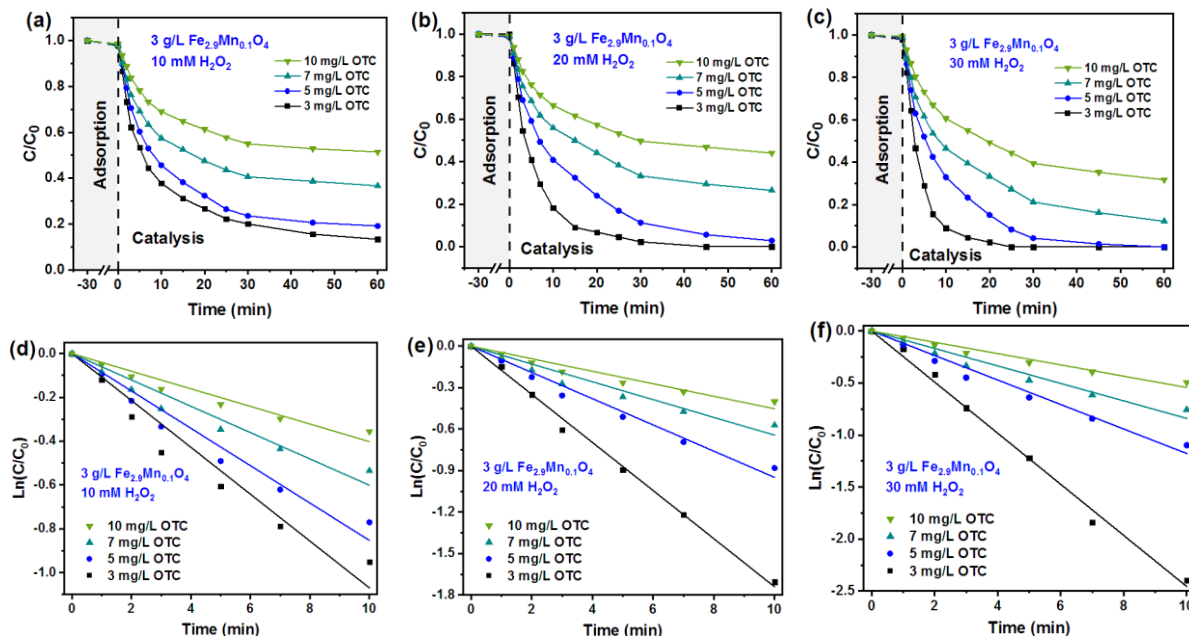


Fig. 8. (a-c) Changes of OTC concentration vs. reaction time in the presence of the Mn-10 catalyst at 298 K; (d-f) first-order kinetic model for the Mn-10 catalyst at 298 K.

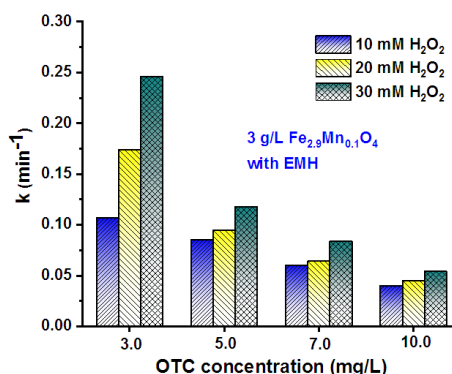


Fig. 9. Rate constants of the first-order kinetic model for the degradation of OTC with the Mn-10.

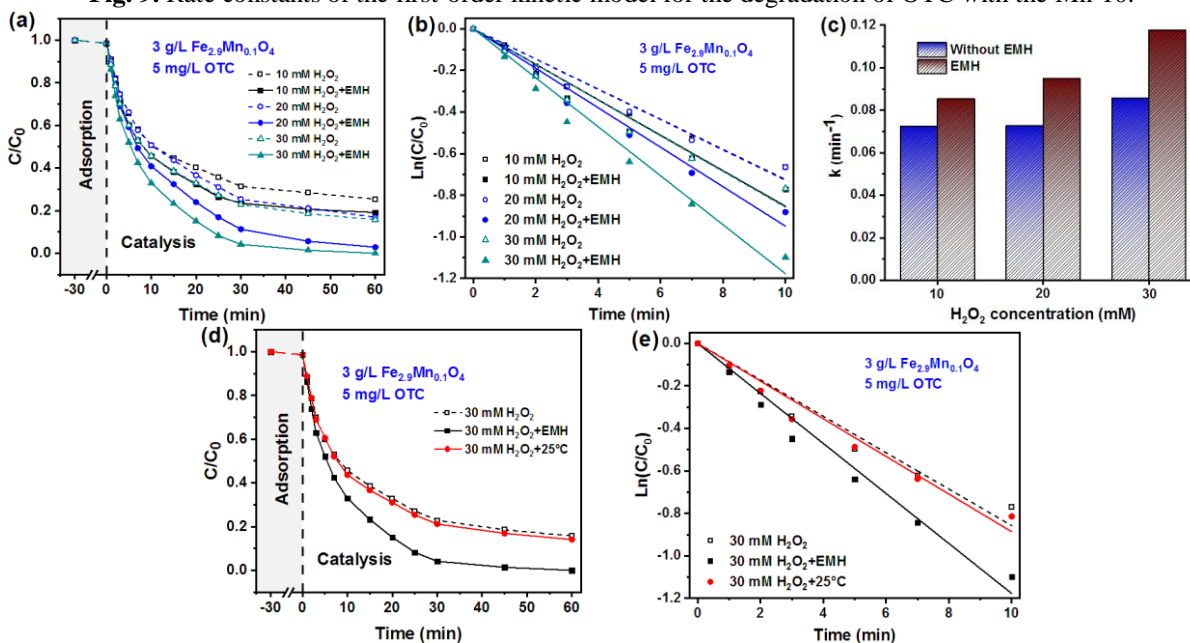


Fig. 10. (a) Catalytic activity of Mn-10 nanoparticles in the OTC decomposition without and under EMH; (b) log-linear transformation of the wet oxidation kinetic lines; (c) rate constants of the first-order kinetic model for the degradation of OTC with the Mn-10; (d) catalytic activity of Mn-10 nanoparticles in the OTC decomposition without EMH, under EMH and with heating to 25°C in a water bath; (e) log-linear transformation of the wet oxidation kinetic lines.

2.4. Catalytic activity in the bacterial inactivation

Figure 11-a displays the results of experiments conducted to determine the antibacterial efficacy of manganese-doped catalysts. The inactivation kinetics of *E. coli* bacteria were studied over a period of 135 minutes. The H₂O₂ concentration was 20 mM. The initial bacterial count was 10⁴ colony-forming units per milliliter (CFU/mL). The catalysts were dosed at a concentration of 1 g/L. The graph illustrates the catalysts with the highest activity levels for compositions of Mn-05, Mn-10, and Mn-15. They aid in water disinfection and reduce the number of Gram-negative bacteria to 38, 36, and 39 CFU/mL, respectively. Samples Mn-02, Mn-20, and Mn-25 showed lower antibacterial activity. Control experiments were performed in the presence of hydrogen peroxide and in the presence of catalysts and *E. coli*. Figure 11-b shows the results of catalytic disinfection with [E. coli]₀ = 10⁶ CFU/mL and [H₂O₂]₀ = 20 mM. For comparison, we studied two catalyst doses: 1 g/L and 3 g/L. The study confirmed the expected results regarding the effect of Mn-doped magnetite on water disinfection. The antibacterial effectiveness of catalysts increases as the concentration is raised from 1 g/L to 3 g/L. Samples Mn-05 and Mn-10 destroyed the highest concentration of bacteria. This confirms their high efficacy in eliminating persistent biological pollutants. For example, after 135 minutes of catalytic disinfection, a 1 g/L sample of Mn-05 reduced the amount of *E. coli* from 620000 CFU/mL to 1320 CFU/mL, while 3 g/L of the added oxide eliminated the bacteria from 620000 CFU/mL

to 21 CFU/mL. The inactivation in the presence of H₂O₂ alone was minimal.

Electromagnetic heating can be an effective method for catalytic reactions in aqueous solutions, including water disinfection. Recent studies indicate that the use of nanomaterials in an external magnetic field is highly effective for removing pollutants. Figure 12-a illustrates the experimental results of inactivating Gram-negative bacteria ([*E. coli*]₀ = 10⁶ CFU/mL) without electromagnetic heating and with EMH. The concentration of hydrogen peroxide was 20 mM. After analyzing the results mentioned above, a catalyst weighting of 3 g/L was selected. This weight demonstrated the highest activity in the catalytic reaction of H₂O₂ decomposition. As anticipated, the EMH experiments exhibited superior performance and achieved complete inactivation of *E. coli* bacteria. The results indicate that Mn-02 and Mn-05 catalysts were the most effective, as they eliminated all *E. coli* bacteria after 135 minutes. Mn-10 sample combined with electromagnetic heating, reduces the amount of Gram-negative bacteria in water from 10⁶ CFU/mL to 12 CFU/mL. In contrast, an experiment conducted without electromagnetic heating resulted in a reduction of bacteria to 10² CFU/mL. Pure magnetite (Mn-00) showed a high percentage of Gram-negative bacteria inactivation under the influence of electromagnetic heating. In all experiments, electromagnetic heating resulted in a more efficient decomposition of H₂O₂. The study [17] also observed the acceleration of hydrogen peroxide

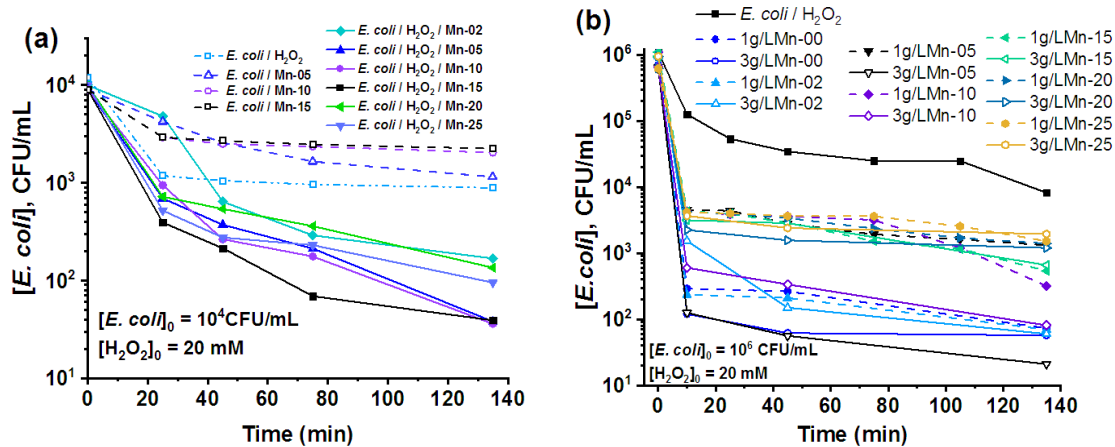


Fig. 11. Effect of Mn-doped magnetite samples on the inactivation of *E. coli*
 (a) [*E. coli*]₀ = 10⁴ CFU/mL (b) [*E. coli*]₀ = 10⁶ CFU/mL.

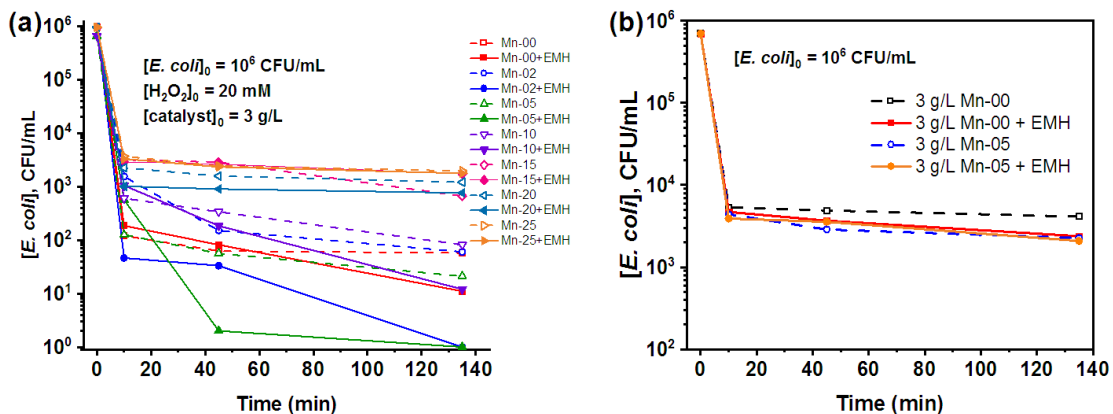


Fig. 12. *E. coli* inactivation in the presence of Fe_{3-x}Mn_xO₄ catalysts and electromagnetic heating.

decomposition through electromagnetic heating. Figure 12-b shows the results of the effect of catalysts without H₂O₂ on microbial organisms. The catalyst adsorbs 2 log of bacteria. The results demonstrate that the synthesized catalysts are highly effective in deactivating persistent biological contaminants.

2.5. Toxicology

Toxicity assessment during pollutant degradation is an important indicator of water treatment efficiency. Biotests are conducted to obtain information on the safety of a proposed method of contaminated water treatment. In this work, the acute ecotoxicity after the Fenton process was evaluated using *D. magna* neonates. Water toxicity analysis was performed after the inactivation process of 10⁶ CFU/mL bacteria in the presence of 20 mM H₂O₂ and synthesized catalysts (3 g/L). The results of the biological analysis showed that water contaminated with residual concentration of H₂O₂ is toxic [31]. H₂O₂ molecules can be hazardous to the environment due to their acute toxicity. However, their efficient decomposition can produce water that is safe for consumption. A comparison of the residual H₂O₂ concentration obtained from chemical analysis and the results of biological analysis using a bioindicator showed that *D. magna* is a reliable tool for determining the efficiency and safety of the Fenton process. It is important to note that the use of catalysts can significantly affect the process. Mn-00, Mn-02, Mn-05, Mn-10, Mn-15, Mn-20, and Mn-25 showed different levels of activity; the hydrogen peroxide concentration reached different levels after 90 minutes.

The mortality of *D. magna* organisms was found to be independent of the concentration of *E. coli* bacteria based on biological analysis. The EC₅₀ for the oxytetracycline solution was 102 mg/L after 48 hours. Therefore, the primary factor affecting water toxicity was the residual concentration of H₂O₂. Figure 13 shows the changes in

residual H₂O₂ concentration as a function of the stoichiometric ratio of Mn²⁺/Fe²⁺. The efficiency of hydrogen peroxide removal increased to 100% as the Mn²⁺ content in magnetite increased. In addition, 100% survival rate of *Daphnia magna* was observed.

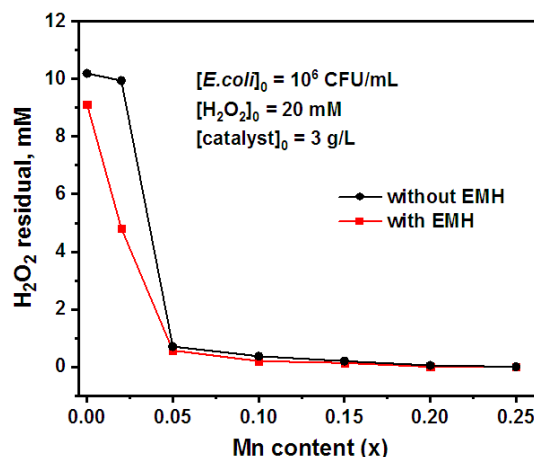


Fig. 13. The correlation between the residual H₂O₂ concentration and Mn²⁺ content in magnetite (conditions: [*E. coli*]₀ = 10⁶ CFU/mL; [catalyst]₀ = 3 g/L; [H₂O₂]₀ = 20 mM).

The EC₅₀ concentration of H₂O₂, that resulted in 50% mortality of *D. magna* at 24 and 48 hours, was calculated based on the biological analysis. With electromagnetic heating, the EC₅₀ for 24 and 48 hours was 0.775 and 0.510 mM H₂O₂, respectively. Without the use of electromagnetic heating, the EC₅₀ values for 24 and 48 hours were 0.762 and 0.360 mM H₂O₂, respectively. The ability of the synthesized Fe_{3-x}Mn_xO₄ samples' to inactivate bacteria and reduce water toxicity increases with higher Mn²⁺ content in the composite, as shown by the biological analysis (Fig. 14 a,c). Samples Mn-00 and Mn-02 showed the highest toxicity of purified water,

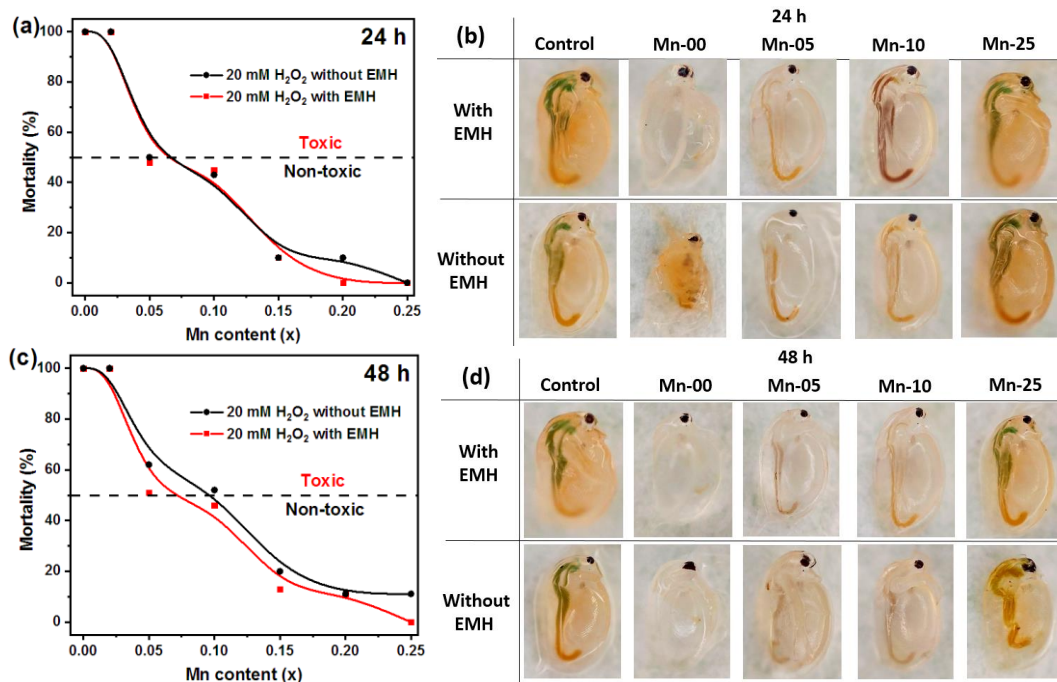


Fig. 14. Mortality of *D. magna* population at different of catalyst with EMH and without EMH: (a) 24 hours and (c) 48 hours; morphology of *Daphnia magna* exposed to treated water: (b) 24 hours and (d) 48 hours.

resulting in 100% mortality of *D. magna* organisms. After 48 hours, the internal organs of the test animals' were severely damaged, leaving them as empty shells (Fig. 14d). For the most active samples, Mn-05 and Mn-10, mortality rates of 47.6% and 44.9%, respectively, were observed within 24 hours. Sample Mn-25 showed the least amount of toxicity during bacterial inactivation. The residual concentration of hydrogen peroxide was 0 mM, and no visible effects on *D. magna* organisms were observed (Fig. 14b,d). The data suggest that the toxicity of the treated water decreased with the degradation of H₂O₂.

Conclusions

Fe_{3-x}Mn_xO₄ (x = 0.0; 0.02; 0.05; 0.1; 0.15; 0.2; 0.25) catalysts with high magnetic properties were synthesized using the co-precipitation method. The sample Mn-05 showed the highest activity for the activation of H₂O₂ in the degradation of OTC and *E. coli* bacteria. The removal rate of OTC (3 mg/L) increased gradually as the concentration of H₂O₂ increased from 10 to 30 mM. The reaction efficiency increased when the solution temperature was raised to 25°C using electromagnetic heating. Electromagnetic heating improved catalytic properties. The decomposition efficiency of 5 mg/L OTC by the Mn-10 sample with EMH, without electromagnetic heating, and with water heating was 100, 84.3, and 86.1 %, respectively. Mn-05, Mn-10, and Mn-15 are the most effective catalysts for water disinfection and reducing the number of Gram-negative bacteria. Studies on ecotoxicity have shown that *D. magna* is a sensitive bioindicator of residual H₂O₂ concentration. With electromagnetic heating, the EC₅₀ for 24 and 48 hours was 0.775 and

0.510 mM H₂O₂, respectively. An increase in the Mn²⁺ content in the synthesized catalysts resulted in a decrease in the toxicity of purified water. Biotests are a cost-effective and simple alternative to physicochemical analysis. Fe_{3-x}Mn_xO₄ catalysts can be used for the catalytic decomposition of OTC and inactivation of *E. coli* bacterium with H₂O₂.

Acknowledgment

The authors thank the Ministry of Education and Science of Ukraine for financial support in the framework of project number 0121U109476 ("Engineering of metal oxide catalysts with the regulating activity function for water disinfection with hydroxyl radicals", 2021-2023).

Danyliuk Nazarrii – PhD student, leading specialist at the Educational and Scientific Center of Material Science and Nanotechnology, Vasyl Stefanyk Precarpathian National University;

Lapchuk Ivanna – PhD student, leading specialist at the Educational and Scientific Center of Material Science and Nanotechnology, Vasyl Stefanyk Precarpathian National University;

Kotsyubynsky Volodymyr – Professor of the Department of Materials Science and New Technologies, Vasyl Stefanyk Precarpathian National University;

Boychuk Volodymyra – Professor of the Department of Materials Science and New Technologies, Vasyl Stefanyk Precarpathian National University;

Husak Viktor – Associate Professor of the Biochemistry and Biotechnology Department, Vasyl Stefanyk Precarpathian National University.

- [1] S. Rahim Pouran, A.A. Abdul Raman, W.M.A. Wan Daud, *Review on the application of modified iron oxides as heterogeneous catalysts in Fenton reactions*, J. Clean. Prod. 64, 24 (2014); <https://doi.org/10.1016/j.jclepro.2013.09.013>.
- [2] E.M.R. Rocha, V.J.P. Vilar, A. Fonseca, I. Saraiva, R.A.R. Boaventura, *Landfill leachate treatment by solar-driven AOPs*, Sol. Energy. 85, 46 (2011); <https://doi.org/10.1016/j.solener.2010.11.001>.
- [3] X. Wang, L. Zhang, *Kinetic study of hydroxyl radical formation in a continuous hydroxyl generation system*, RSC Adv. 8, 40632(2018); <https://doi.org/10.1039/C8RA08511K>.
- [4] C. Ruales-Lonfat, J.F. Barona, A. Sienkiewicz, M. Bensimon, J. Vélez-Colmenares, N. Benítez, C. Pulgarín, *Iron oxides semiconductors are efficient for solar water disinfection: A comparison with photo-Fenton processes at neutral pH*, Appl. Catal. B Environ. 166–167, 497 (2015); <https://doi.org/10.1016/j.apcatb.2014.12.007>.
- [5] S. Natarajan, K. Harini, G.P. Gajula, B. Sarmiento, M.T. Neves-Petersen, V. Thiagarajan, *Multifunctional magnetic iron oxide nanoparticles: diverse synthetic approaches, surface modifications, cytotoxicity towards biomedical and industrial applications*, BMC Mater. 1, 1 (2019); <https://doi.org/10.1186/s42833-019-0002-6>.
- [6] G. Sathishkumar, V. Logeshwaran, S. Sarathbabu, P.K. Jha, M. Jeyaraj, C. Rajkuberan, N. Senthilkumar, S. Sivaramakrishnan, *Green synthesis of magnetic Fe₃O₄ nanoparticles using Couroupita guianensis Aubl. fruit extract for their antibacterial and cytotoxicity activities*, Artif. Cells, Nanomedicine Biotechnol. 46, 589 (2018); <https://doi.org/10.1080/21691401.2017.1332635>.
- [7] K. Hanna, T. Kone, G. Medjahdi, *Synthesis of the mixed oxides of iron and quartz and their catalytic activities for the Fenton-like oxidation*, Catal. Commun. 9, 955 (2008); <https://doi.org/10.1016/j.catcom.2007.09.035>.
- [8] H.H. Huang, M.C. Lu, J.N. Chen, *Catalytic decomposition of hydrogen peroxide and 2-chlorophenol with iron oxides*, Water Res. 35, 2291 (2001); [https://doi.org/10.1016/S0043-1354\(00\)00496-6](https://doi.org/10.1016/S0043-1354(00)00496-6).
- [9] J. Du, J. Bao, Y. Liu, S.H. Kim, D.D. Dionysiou, *Facile preparation of porous Mn/Fe₃O₄ cubes as peroxydisulfate activating catalyst for effective bisphenol A degradation*, Chem. Eng. J. 376, 119193 (2019); <https://doi.org/10.1016/j.cej.2018.05.177>.
- [10] Y. Li, J. He, K. Zhang, P. Hong, C. Wang, *Oxidative degradation of sulfamethoxazole antibiotic catalyzed by porous magnetic manganese ferrite nanoparticles: mechanism and by-products identification*, J. Mater. Sci. 55, 13767 (2020); <https://doi.org/10.1007/s10853-020-05000-y>.

- [11] X. Peng, J. Qu, S. Tian, Y. Ding, X. Hai, B. Jiang, *Green fabrication of magnetic recoverable graphene/MnFe₂O₄ hybrids for efficient decomposition of methylene blue and the Mn/Fe redox synergetic mechanism*, RSC Adv. 6, 104549 (2016); <https://doi.org/10.1039/C6RA24320G>.
- [12] C. Lai, F. Huang, G. Zeng, D. Huang, L. Qin, M. Cheng, C. Zhang, B. Li, H. Yi, S. Liu, L. Li, *Fabrication of novel magnetic MnFe₂O₄/bio-char composite and heterogeneous photo-Fenton degradation of tetracycline in near neutral pH*, Chemosphere. 224, 910 (2019); <https://doi.org/10.1016/j.chemosphere.2019.02.193>.
- [13] Z. Chen, Y. Zheng, Y. Liu, W. Zhang, Y. Wang, X. Guo, X. Tang, Y. Zhang, Z. Wang, T. Zhang, *Magnetic Mn-Doped Fe₃O₄ hollow Microsphere / RGO heterogeneous Photo-Fenton Catalyst for high efficiency degradation of organic pollutant at neutral pH*, Mater. Chem. Phys. 238, 121893 (2019); <https://doi.org/10.1016/j.matchemphys.2019.121893>.
- [14] G.X. Huang, C.Y. Wang, C.W. Yang, P.C. Guo, H.Q. Yu, *Degradation of bisphenol a by peroxymonosulfate catalytically activated with Mn_{1.8}Fe_{1.2}O₄ Nanospheres: Synergism between Mn and Fe*, Environ. Sci. Technol. 51, 12611 (2017); <https://doi.org/10.1021/acs.est.7b03007>.
- [15] F. Ameen, A. Aygun, A. Seyrankaya, R.N. Elhouda Tiri, F. Gulbagca, İ. Kaynak, N. Majrashi, R. Orfali, E.N. Dragoi, F. Sen, *Photocatalytic investigation of textile dyes and E. coli bacteria from wastewater using Fe₃O₄@MnO₂ heterojunction and investigation for hydrogen generation on NaBH₄ hydrolysis*, Environ. Res. 220, 115231 (2023); <https://doi.org/10.1016/j.envres.2023.115231>.
- [16] T. Tatarchuk, N. Danyliuk, I. Lapchuk, W. Macyk, A. Shyichuk, R. Kutsyk, V. Kotsyubynsky, V. Boichuk, *Oxytetracycline removal and E. Coli inactivation by decomposition of hydrogen peroxide in a continuous fixed bed reactor using heterogeneous catalyst*, J. Mol. Liq. 366, 120267 (2022); <https://doi.org/10.1016/j.molliq.2022.120267>.
- [17] T. Tatarchuk, A. Shyichuk, N. Danyliuk, M. Naushad, V. Kotsyubynsky, V. Boychuk, *Cobalt ferrite as an electromagnetically boosted metal oxide hetero-Fenton catalyst for water treatment*, Chemosphere. 326, 138364 (2023); <https://doi.org/10.1016/j.chemosphere.2023.138364>.
- ISO 6341:2012 Water quality - Determination of the inhibition of the mobility of Daphnia magna Straus (Cladocera, Crustacea) - Acute toxicity test, BSI Stand. Publ. (2012).
- [18] J. Li, H. Yuan, G. Li, Y. Liu, J. Leng, *Cation distribution dependence of magnetic properties of solgel prepared MnFe₂O₄ spinel ferrite nanoparticles*, J. Magn. Mater. 322, 3396 (2010); <https://doi.org/10.1016/j.jmmm.2010.06.035>.
- [19] C. Simon, A. Blösser, M. Eckardt, H. Kurz, B. Weber, M. Zobel, R. Marschall, *Magnetic properties and structural analysis on spinel MnFe₂O₄ nanoparticles prepared via non-aqueous microwave synthesis*, Zeitschrift Fur Anorg. Und Allg. Chemie. 647, 2061 (2021); <https://doi.org/10.1002/zaac.202100190>.
- [20] T. Tatarchuk, N. Danyliuk, A. Shyichuk, V. Kotsyubynsky, I. Lapchuk, *Green synthesis of cobalt ferrite using grape extract: the impact of cation distribution and inversion degree on the catalytic activity in the decomposition of hydrogen peroxide*, Emergent Mater. 5, 89 (2021); <https://doi.org/10.1007/s42247-021-00323-1>.
- [21] M. Czaja, R. Lisiecki, R. Juroszek, T. Krzykawski, *Luminescence properties of tetrahedral coordinated Mn²⁺; genthelvite and willemite examples*, Minerals. 11, 1215 (2021); <https://doi.org/10.3390/min11111215>.
- [22] K.S.A. Kumar, R.N. Bhowmik, S.H. Mahmood, *Role of pH value during chemical reaction, and site occupancy of Ni²⁺ and Fe³⁺ ions in spinel structure for tuning room temperature magnetic properties in Ni_{1.5}Fe_{1.5}O₄ ferrite*, J. Magn. Mater. 406, 60 (2016); <https://doi.org/10.1016/j.jmmm.2015.12.100>.
- [23] R. Zapukhlyak, M. Hodlevsky, V. Boychuk, J. Mazurenko, V. Kotsyubynsky, L. Turovska, B. Rachiy, S. Fedorchenko, *Structure and magnetic properties of hydrothermally synthesized CuFe₂O₄ and CuFe₂O₄/rGO composites*, J. Magn. Mater. 587, 171208 (2023); <https://doi.org/10.1016/j.jmmm.2023.171208>.
- [24] R.S. De Biasi, L.H.G. Cardoso, *A simple model for the magnetocrystalline anisotropy in mixed ferrite nanoparticles*, Phys. B Phys. Condens. Matter. 407, 3893 (2012); <https://doi.org/10.1016/j.physb.2012.06.017>.
- [25] C. Iacovita, A. Florea, L. Scorus, E. Pall, R. Dudric, A.I. Moldovan, R. Stiufiuc, R. Tetean, C.M. Lucaciu, *Hyperthermia, cytotoxicity and cellular uptake properties of manganese and zinc ferrite magnetic nanoparticles synthesized by a polyol-mediated process*, Nanomaterials. 9, 1489 (2019); <https://doi.org/10.3390/nano9101489>.
- [26] B.D. Cullity, C.D. Graham, *Introduction to magnetic materials*, John Wiley Sons. (2011); <https://doi.org/10.1002/9780470386323>.
- [27] P. García-Negueroles, S. García-Ballesteros, A.M. Amat, E. Laurenti, A. Arques, L. Santos-Juanes, *Unveiling the Dependence between Hydroxyl Radical Generation and Performance of Fenton Systems with Complexed Iron*, ACS Omega. 4, 21698 (2019); <https://doi.org/10.1021/acsomega.9b02241>.
- [28] Y.D. Dong, Y. Shi, Y.L. He, S.R. Yang, S.Y. Yu, Z. Xiong, H. Zhang, G. Yao, C.S. He, B. Lai, *Synthesis of Fe-Mn-Based Materials and Their Applications in Advanced Oxidation Processes for Wastewater Decontamination: A Review*, Ind. Eng. Chem. Res. 62, 10828 (2023); <https://doi.org/10.1021/acs.iecr.3c01624>.
- [29] S. Anothairungrat, S. Ouajai, K. Piyamongkala, *Screening Test of Evaluation Thermal Hazard for H₂O₂ by DSC*, IOP Conf. Ser. Earth Environ. Sci. 219, 012017 (2019); <https://doi.org/10.1088/1755-1315/219/1/012017>.
- [30] E.S. Reichwaldt, L. Zheng, D.J. Barrington, A. Ghadouani, *Acute Toxicological Response of Daphnia and Moina to Hydrogen Peroxide*, J. Environ. Eng. 138, 607 (2012); [https://doi.org/10.1061/\(asce\)ee.1943-7870.0000508](https://doi.org/10.1061/(asce)ee.1943-7870.0000508).

Назарій Данилюк¹, Іванна Лапчук¹, Володимир Коцюбинський²,
Володимира Бойчук², Віктор Гусак³

Вплив заміщення Mn^{2+} на каталітичні властивості наночастинок $Fe_{3-x}Mn_xO_4$, синтезованих методом співосадження

¹Навчально-науковий центр матеріалознавства і нанотехнологій, Прикарпатський національний університет імені Василя Стефаника, Івано-Франківськ, Україна, danyliuk.nazariy@gmail.com

²Кафедра матеріалознавства та нових технологій, Прикарпатський національний університет імені Василя Стефаника, Івано-Франківськ, Україна, kotsyubynsky@gmail.com

³Кафедра біохімії та біотехнологій, Прикарпатський національний університет імені Василя Стефаника, Івано-Франківськ, Україна, gus_net@ukr.net

Mn-заміщені каталізатори $Fe_{3-x}Mn_xO_4$ (де $x = 0.0; 0.02; 0.05; 0.1; 0.15; 0.2; 0.25$), синтезовано методом співосадження. X-променеві дифрактограми підтвердили утворення чистого, добре закристалізованого фериту мангану із кубічною структурою шпінелі. Розмір кристалітів різко зростає для мінімальних ступенів заміщення іонів Mn^{2+} на Fe^{2+} , з подальшою тенденцією зменшення. В роботі досліджено каталітичні властивості $Fe_{3-x}Mn_xO_4$ щодо деградації антибіотику окситетрацикліну (ОТС) та інактивації бактерій *E. coli*. Спостерігається кореляція між розміром частинок і каталітичною активністю. Зразок $Fe_{2.95}Mn_{0.05}O_4$ проявив найвищу каталітичну активність (ступінь деградації ОТС становить 86,76%). Досліджено вплив електромагнітного нагріву (ЕМН) на каталітичні властивості синтезованих каталізаторів. Каталізатор $Fe_{2.9}Mn_{0.1}O_4$ під дією електромагнітного нагріву досягав 100% ефективності при розкладі 5 мг/л ОТС. Зразки $Fe_{3-x}Mn_xO_4$ ефективно зменшують кількість грам-негативних бактерій *E. coli* (10^4 і 10^6 КУО/мл). Експерименти в присутності електромагнітного нагріву продемонстрували високу ефективність інактивації бактерій *E. coli* за допомогою каталізаторів $Fe_{2.98}Mn_{0.02}O_4$ і $Fe_{2.95}Mn_{0.05}O_4$ впродовж 135 хвилин. Дослідження екотоксичності показали, що *Daphnia magna* є чутливим біоіндикатором до залишкової концентрації H_2O_2 . Збільшення вмісту Mn^{2+} у синтезованих каталізаторах призводить до зниження токсичності очищеної води. Проведене дослідження дозволяє припустити, що Mn-заміщені магнетитові каталізатори є ефективними матеріалами для розкладу ОТС та інактивації бактерій *E. coli*.

Ключові слова: каталізатор, Mn-заміщений магнетит, пероксид водню, електромагнітний нагрів, *E. coli*, *Дафнія магна*.